*Int. J. Electrochem. Sci.*, 9 **(2014)** 2859 - 2866

International Journal of
ELECTROCHEMICAL
SCIENCE
www.electrochemsci.org

# Copper Oxide Hierarchical Microspheres Grown on Copper Foil and Their Enhanced Performance as Anodes for Li-ion Batteries

*Shasha Jin*[1,*], *Xiaobo Zhu*[1], *and Yitai Qian*[1,2]

[1] Hefei National Laboratory for Physical Science at Microscale and Department of Chemistry, University of Science and Technology of China, Hefei, Anhui 230026, PR China
[2] Key Laboratory of Colloid and Interface Chemistry (Shandong University), Ministry of Education, and School of Chemistry and Chemical Engineering, Shandong University, Jinan 250100, PR China
[*]E-mail: XX-YY

*Received:* 21 January 2014 / *Accepted:* 13 February 2014 / *Published:* 23 March 2014

Here copper oxide hierarchical microspheres directly grown on copper foil are achieved through a hydrothermal reaction. By changing the reaction temperature from 100 °C to 150 °C, the CuO nanostructures respectively present as urchin-like architectures assembled by nanorods and hollow microspheres composed of nanoparticles, which are confirmed by their scanning electron microscopy images. Then the resultant CuO@Cu organizers are directly served in Li-ion batteries without any binders and conductive additives. Hence, the copper foil performs as both the supporter of CuO formation and the current collector of the electrodes. Correspondingly, urchin-like CuO spheres@Cu deliver the combination of good rate and excellent cycle performance, which receive capacity of 250 mA h $g^{-1}$ at 2 Ah $g^{-1}$ and maintain a high reversible capacity of 600 mA h $g^{-1}$ even after 400 cycles at 100 mAh $g^{-1}$

**Keywords:** Li-ion batteries; copper oxide; hierarchical microspheres; copper foil supporter.

## 1. INTRODUCTION

Lithium ion batteries (LIBs) have been considered as the most promising power sources for future electric vehicles. To meet the future demand for their applications in future electric vehicles, electrodes with high specific energy density, durability, cost, and intrinsic safety are required. Comparing to commercially used graphite (372 mAh $g^{-1}$), transition metal oxides ($M_xO_y$, M = Fe,[1] Co,[2] Ni,[3] Mn,[4] Cu,[5] etc.) have much higher theoretic capacity and better rate performance, which have been extensively investigated as potential anode materials thereby replacing carbonaceous anodes for next-generation LIBs. Among them, CuO has been considered as a promising candidate as

an anode material due to its high specific capacity (670 mA h $g^{-1}$), abundance of raw, low cost, non-toxicity, easily production, and environmental friendliness. [6]

However, the oxides powders often suffer from some limitations such as poor electronic conductivity; moreover, large volume change of MO particles during reaction with $Li^+$ ions often results in the pulverization and strong polarization of the electrodes, which prevents them from being used in large commercial application.[7-9] Therefore, it is necessary to solve these problems to meet new needs in future as anode materials. Up to now, many efforts have been made to improve the electrochemical performance of CuO materials. Among them, synthesis of carbon-assisted composites, for instance, graphene and CNT, [7, 10-13] is considered as an important route. Practically, the introduction of carbon can improve the electronic conductivity and relieve the volume variation during $Li^+$ insertion/extraction. But these methods may lead to loss of overall specific capacity of the products and the modifications often appear to be complex, involving added multiple steps.

Apart from introduction of carbon, using nanoarchitectured electrodes has attracted considerable attention since they allow for enhanced electronic conductivity and accommodation of the strain of lithium uptake/release without compensation of ratio of active materials.[14] Morales et al. [15] have prepared nanostructured CuO thin films by spray-pyrolysis method, and found that the nanostructured CuO electrodes could deliver a reversible capacity as high as 625 mAh $g^{-1}$ up to 100 cycles. Wang et al.[16] demonstrated that the electrode of CuO with dandelion-like hollow microspheres could release a reversible capacity more than 600 mAh $g^{-1}$ up to 50 cycles. Yang et al. [17] have fabricated CuO nanotube film electrode which demonstrated a reversible capacity over 417 mAh $g^{-1}$ up to 30 cycles. Notably, for the fabrication of a traditional LIB electrode, CuO nanostructures need to be mixed with a polymeric binder and carbon black and further pressed onto the current collector. This process suffers from poor electron transport due to additional undesirable interfaces, unfavorable accessibility to active materials, and lowered specific capacity caused by the extra weight of additives.[18] It is noteworthy that some one-dimensional (1D) nanostructure array grown directly on a current collector can effectively overcome the drawbacks and exhibit superior rate performance.[19] In this regard, a binder-free CuO electrode is suggested to be a promising anode which should be investigated.

Herein, we integrate the additive-free design and nanostructure merits through employing copper foil supported CuO nanostructures, which are originated from one-pot hydrothermal reactions at different temperatures. Among them, well-shaped urchin-like CuO hollow spheres are determined to deliver better electrochemical performance after examining as anodes of LIBs, which achieve a high discharge capacity of 994.8 mA h $g^{-1}$ for 60 cycles at 100 mA $g^{-1}$, and receive 400 mA h $g^{-1}$ even at 1000 mA $g^{-1}$.

## 2. EXPERIMENTAL SECTION

### *2.1. Sample Preparation.*

All of the reagents used were analytical grade purity without further purification. In a typical procedure, 0.3 g cupric acetate and 1.8 g PEG-20000 were dissolved in 20 mL of distilled water,

respectively. Then the two solutions were mixed together and transferred to 50 mL stainless steel Teflon lined autoclaves coupled with Cu metal foil. Next, the autoclaves are sealed and maintained respectively at 100 and 150 °C for 10 h. Finally, products supported by copper foil are obtained after being washed with distilled water and absolute ethanol for three times and dried in vacuum at 60 °C for 4 h, namely C100 and C150.

### *2.2. Characterization*

The as-prepared products stripped off from the Cu foil were characterized by powder X-ray diffraction (XRD) on a Philips X'pert X-ray diffractometer equipped with Cu Ka radiation (l - 1.5418Å). The morphologies of the samples on Cu foil were directly examined using field-emission scanning electron microscopy (FESEM, JEOL JSM-6700F).

### *2.3. Electrochemical measurements*

Charge / discharge tests were carried out using coin-type cells (size: 2016), which consisted of an active material working electrode and a Li foil counter electrode separated by a Celgard 2300 microporous membrane. Obtained copper foil supported CuO nanosturctures are directly employed as working electrode after being dried and pressed into wafer. And the mass of the active material are determined by the quality change over the hydrothermal reaction. 1 mol/L solution of $LiPF_6$ dissolved in ethylene carbonate/dimethyl carbonate (EC/DMC) (1:1 volume ratio) was used as the electrolyte. The cells were assembled in an argon-filled glove box (Mikrouna, Super 1220/750/900, China). The charge–discharge tests were performed on a LAND battery test system (LAND, CT2001A) in the range of 0.1-3.0 V (vs $Li/Li^+$) at different rates.

## 3. RESULTS AND DISCUSSION

The XRD (X-ray powder diffraction) patterns of the samples are shown in Fig. 1. All of the peaks of the two products can be indexed to pure CuO of a monoclinic structure with lattice parameters *a*) 4.662 Å, *b*) 3.416 Å, *c*) 5.118 Å, and 93.500° (JCPDS card no. 65-2309).[16] Notably, the diffraction peaks of CuO evidently sharpened when the reaction temperature increased from 100 to 150 °C, which indicates an increase of crystallinity with the reaction temperature due to the ordering of the local structure and/or release of the lattice strain.

The SEM (scanning electron microscopy) images of the products are shown in Fig. 2. From the panoramic perspective (Fig 2a, d), microspheres in C100 are more densely compacted together and evenly covered the Cu foil. In strong contrast, the microspheres in C200 are much sparser on the Cu foil thereby presenting as separate microspheres which have clear outline. According to the magnified image of the spheres shown in Fig. 2b and 2e, nevertheless both of the microspheres in C100 and C150

have a diameter of ~2 $\mu$m and rough surface, they have evidently different exterior texture. More exactly, the microsphere in C100 is composed of dense needle-like nanocomponents.

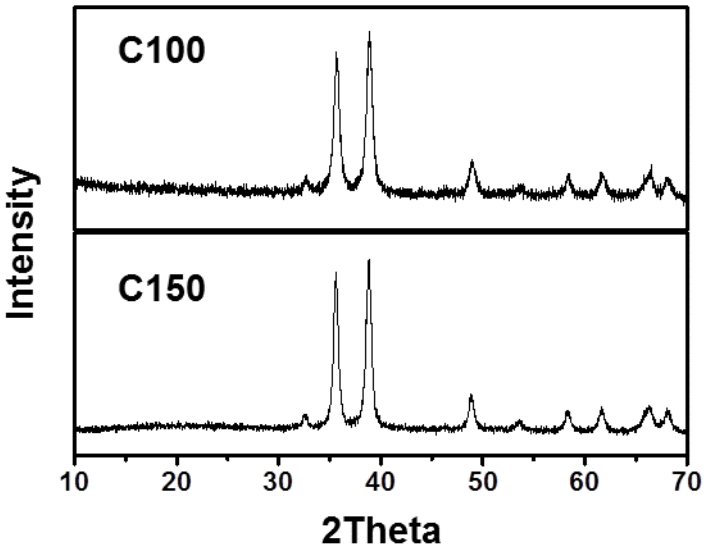


**Figure 1.** XRD pattern of C100 and C150

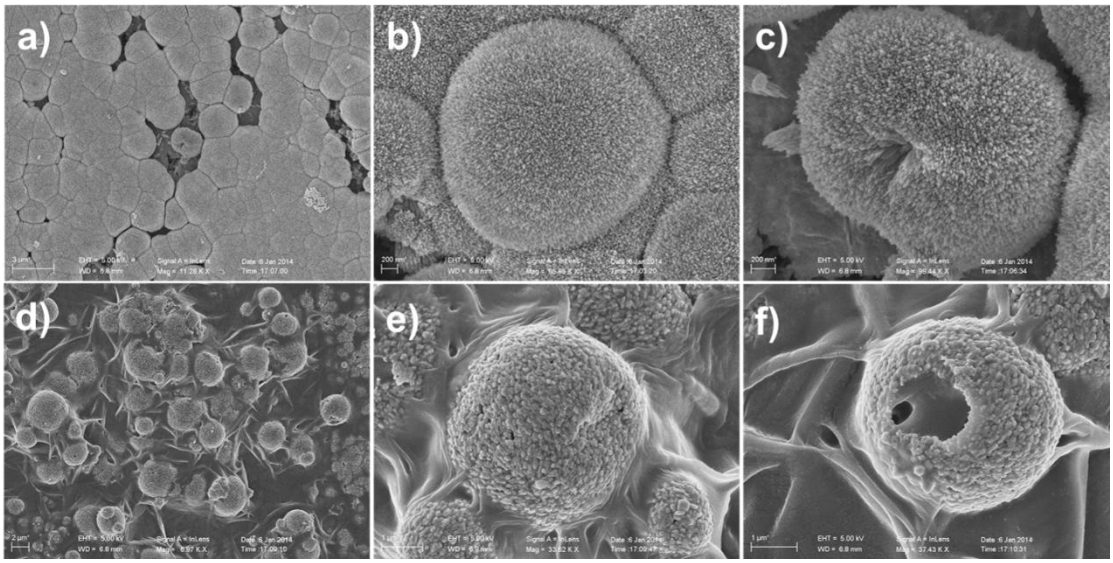


**Figure 2.** SEM images under different magnifications of C100 (a, b, c) and C150 (d, e, f)

In comparison, the surface of microsphere in C150 is constructed by much larger and sparser nanoparticles instead. The observations of broken spheres can also provide differences of the microstructure of the two types of CuO spheres (Fig. 2c, f). Form a gap in a typical broken microsphere of C100, we can convince that such microspheres are closely assembled by numerous needle-like nanocomponents. Interestingly, the magnified image of a typical broken microsphere in

C150 provides intuitionistic evidence of the hollow structure that the diameter of the outer shell is around 400nm coupled with empty interior.

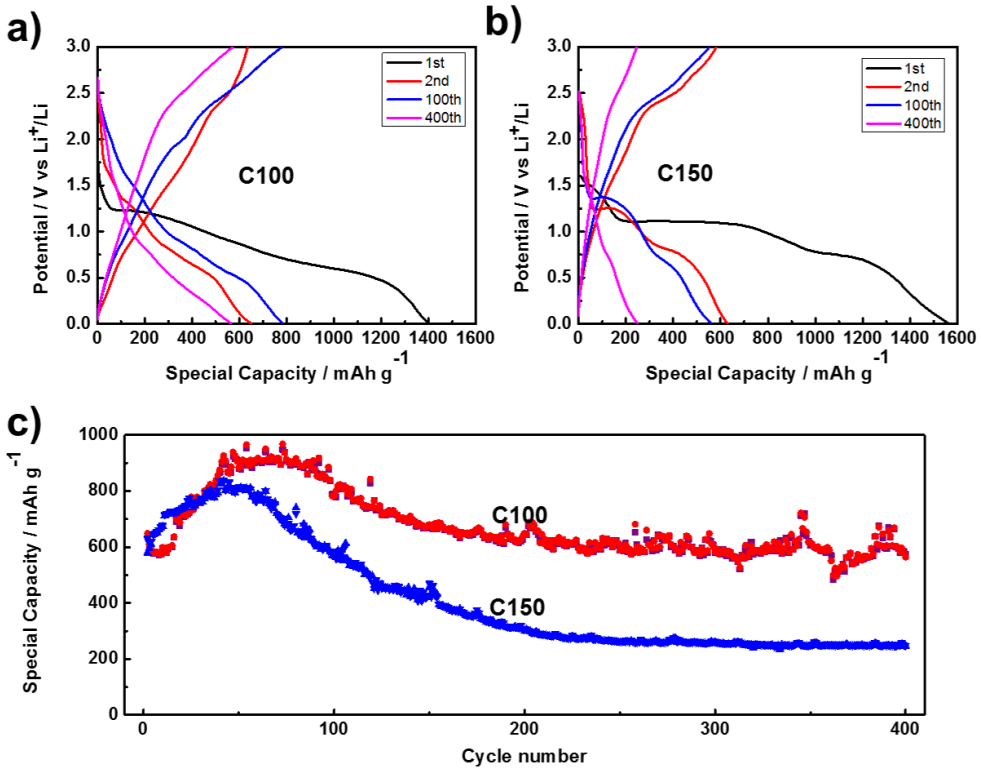


**Figure 3.** Charge-discharge curves (a, b) of C100 and C150 at 100 mAh $g^{-1}$. Cycling capacities of the two products at 100 mAh $g^{-1}$ for 400 cycles.

In order to evaluate the cycle performance of copper foil supported CuO microspheres, they are assembled in LIBs coupled with Li metal then respectively charged and discharged at 100 mA $g^{-1}$. The results are shown in Fig. 3. According to the charge-discharge profiles of C100 (Fig. 3a) and C150 (Fig. 3b), In their first discharge curves, there are three sloping potential ranges of 1.6–1.2, 1.2–0.9 and 0.9–0.01 V, which corresponds to a multi-step electrochemical reaction of CuO related to the creation of a $Cu(II)_{1-x}Cu(I)_xO_{1-x/2}$ solid solution, a $Cu_2O$ phase, reduction to Cu and $Li_2O$, and the growth of the organic SEI (solid electrolyte interface) layers, as discussed in the literature. [16, 20] The electrochemical equations are shown below:

$$CuO + xLi^+ + xe^- \rightarrow Cu(II)_{1-x}Cu(I)_xO_{1-x/2} + x/2\ Li_2O \quad (1)$$

$$Cu(II)_{1-x}Cu(I)_xO_{1-x/2} + (1-x)Li^+ + (1-x)e^- \rightarrow 1/2Cu_2O + (1-x)/2\ Li_2O \quad (2)$$

$$1/2Cu_2O + Li^+ + e^- \rightarrow Cu + 1/2Li_2O \quad (3)$$

In the subsequent cycles, the shapes of the curves of C100 do not change significantly throughout hundreds of cycles indicating excellent capacity retention, while the profiles of C150 experience an evident shrinkage. In particular, C100 and C150 respectively exhibit 780.5 and 574.4 mAh $g^{-1}$ at 100$^{th}$ cycle and 594.1 and 248 m $Ahg^{-1}$ at 400$^{th}$ cycle. Fig. 3c gives a clear illustration of

their charge-discharge capacities variation over the 400 cycle. Before 60 cycles, they have a period of capacity rising. More exactly, C100 reaches discharge capacity of 967 mAh $g^{-1}$ at 73$^{th}$ cycle and C150 receives 873.1 mAh $g^{-1}$ at its 42$^{th}$ discharge. Such capacity rising phenomenon is frequently seen in other reports, and it is believed to be contributed by the formation of SEI layer.[16] However, after the peaks, both of them undergo capacity fading, but C100 exhibit better stability than its counterpart as illustrated in their charge-discharge curves.

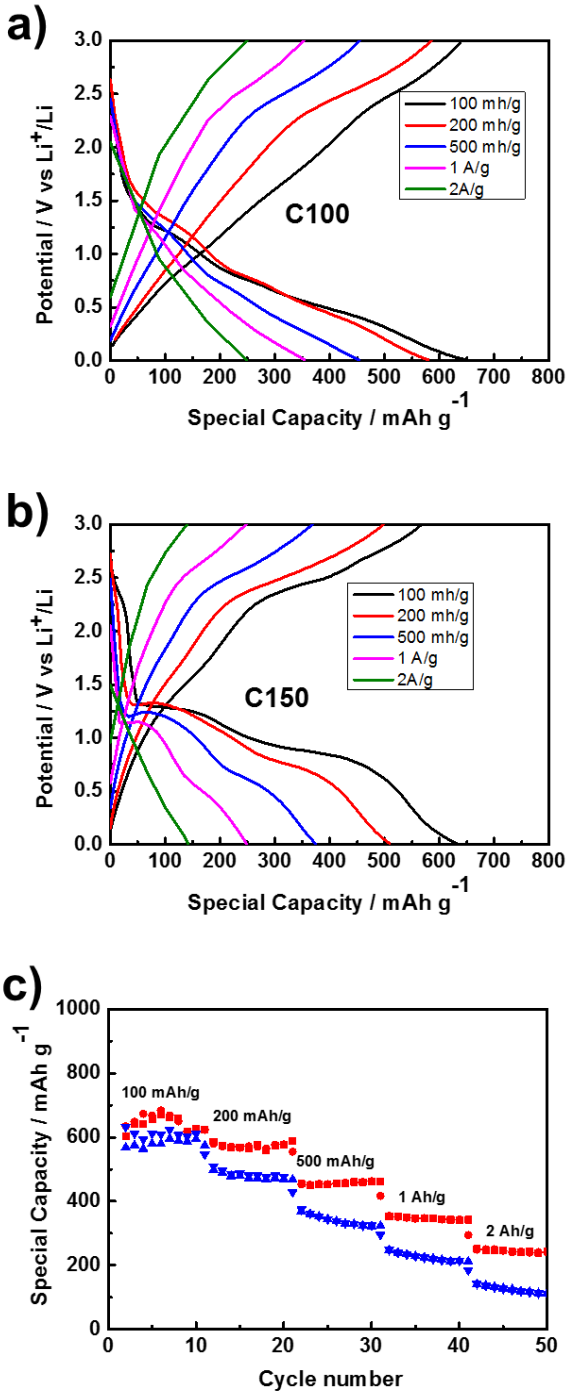


**Figure 4.** Charge-discharge curves (a, b) and capacities (c) of the C100, C150 by discharge sequentially from 100 mAh $g^{-1}$ to 2 Ah $g^{-1}$ for per 10 cycles.

Also, we evaluate the rate performance of the two products conducted under at a series of rates from 100 to 2000 mA $g^{-1}$. Fig. 4a, b show their charge-discharge profiles of every second charge-discharge process of a certain rate. Practically, their rate performance is consistence with their cyclability that C100 exhibits evident advantage over its counterpart. More specifically, at the rates of 100, 200, 500, 1000, and 2000 mA $g^{-1}$, the corresponding discharge capacities are 648.3 to 579.8, 453.2, 354.2, and 248.5 mAh $g^{-1}$ for C100, versus 611.3, 509.2, 428.2, 248.2, and 184.4mAh $g^{-1}$ for C150.

Here the electrochemical measurements indicate that urchin-like CuO spheres @Cu foil can deliver outstanding combination of cycle and rate performance, which are mainly attributed several merits. To begin with, its superiority over C150 indicates the advantage of certain urchin-like morphology, whose nanorods components are much uniform and tinier than the unregular nanoparticles of its counterpart thereby contributing to more efficient contact of active material and electrolyte. Besides, the CuO spheres @Cu foil here demonstrate better cycle stability compared with other similarnanostructured CuO reported, [16, 21, 22] and it is believed that Cu foil supported growth brings about a uniform cover of CuO microspheres on Cu current collector, hence to result in fast electron transfer even without conductive acetylene black.[23] Such strategies are promising for the further development and application.

## 4. CONCLUSIONS

In summary, in this paper we introduce a facile hydrothermal assistant approach to fabricate CuO nanostructures @Cu foil as anodes for LIBs. As confirmed by the scanning electron microscopy images, the CuO nanostructures grown on Cu foil at 100 and 150 °C respectively present as urchin-like architectures assembled by nanorods and hollow microspheres composed of nanoparticles. Then their electrochemical performance of long term cycle and different rate is investigated by directly assembling the products in LIBs without any additives, As a result, urchin-like CuO spheres@Cu deliver the combination of good rate and excellent cycle performance, which receive capacity of 250 mA h $g^{-1}$ at 2 Ah $g^{-1}$ and maintain a high reversible capacity of 600 mA h $g^{-1}$ even after 400 cycles at 100 mAh $g^{-1}$, such performance is attributed to the uniform nanorods formed hierarchical microspheres and the compact contact with Cu current collector. Easy preparation and excellent stability make this Cu supported CuO nanostructures promising for the future generation electrodes. And the development of more efficient deposition of active materials is an area of further research.

ACKNOWLEDGEMENTS
This work was supported by the 973 Project of China (No. 2011CB935901), the National Natural Science Fund of China (No. 91022033, 21201158), Anhui Provincial Natural Science Foundation (1208085QE101)

## References

1. J. Chen, L.-n. Xu, W.-y. Li, X.-l. Gou, *Advanced Materials*, 17 (2005) 582-586.
2. W.-Y. Li, L.-N. Xu, J. Chen, *Advanced Functional Materials*, 15 (2005) 851-857.
3. J. Noda, T. Saku, N. Uchida, *Applied Physics Letters*, 25 (1974) 308-310.

4. J. Gao, M.A. Lowe, H.D. Abruña, *Chemistry of Materials*, 23 (2011) 3223-3227.
5. S. Grugeon, S. Laruelle, R. Herrera-Urbina, L. Dupont, P. Poizot, J.M. Tarascon, *Journal of the Electrochemical Society*, 148 (2001) A285-A292.
6. F.-S. Ke, L. Huang, G.-Z. Wei, L.-J. Xue, J.-T. Li, B. Zhang, S.-R. Chen, X.-Y. Fan, S.-G. Sun, *Electrochimica Acta*, 54 (2009) 5825-5829.
7. S. Ko, J.I. Lee, H.S. Yang, S. Park, U. Jeong, *Advanced Materials*, 24 (2012) 4451-4456.
8. C. Yuan, J. Li, L. Hou, X. Zhang, L. Shen, X.W.D. Lou, *Advanced Functional Materials*, 22 (2012) 4592-4597.
9. X. Chen, N. Zhang, K. Sun, *Journal of Materials Chemistry*, 22 (2012) 13637-13642.
10. S.-F. Zheng, J.-S. Hu, L.-S. Zhong, W.-G. Song, L.-J. Wan, Y.-G. Guo, *Chemistry of Materials*, 20 (2008) 3617-3622.
11. B. Wang, X.-L. Wu, C.-Y. Shu, Y.-G. Guo, C.-R. Wang, *Journal of Materials Chemistry*, 20 (2010) 10661-10664.
12. J.Y. Xiang, J.P. Tu, J. Zhang, J. Zhong, D. Zhang, J.P. Cheng, *Electrochemistry Communications*, 12 (2010) 1103-1107.
13. Y.J. Mai, X.L. Wang, J.Y. Xiang, Y.Q. Qiao, D. Zhang, C.D. Gu, J.P. Tu, *Electrochimica Acta*, 56 (2011) 2306-2311.
14. P.-L. Taberna, S. Mitra, P. Poizot, P. Simon, J.-M. Tarascon, *Nature materials*, 5 (2006) 567-573.
15. J. Morales, L. Sanchez, F. Martin, J.R. Ramos-Barrado, M. Sanchez, *Electrochimica Acta*, 49 (2004) 4589-4597.
16. S.Q. Wang, J.Y. Zhang, C.H. Chen, *Scripta Materialia*, 57 (2007) 337-340.
17. J. Xiang, J. Tu, X. Huang, Y. Yang, *Journal of Solid State Electrochemistry*, 12 (2008) 941-945.
18. L. Qi, S. Chen, Y. Xin, Y. Zhou, Y. Ma, H. Zhou, *Energy & Environmental Science*, (2013).
19. J. Jiang, Y. Li, J. Liu, X. Huang, *Nanoscale*, 3 (2011) 45-58.
20. J. Xiang, J. Tu, L. Zhang, Y. Zhou, X. Wang, S. Shi, *Journal of Power Sources*, 195 (2010) 313-319.
21. S. Gao, S. Yang, J. Shu, S. Zhang, Z. Li, K. Jiang, *Journal of Physical Chemistry* C, 112 (2008) 19324-19328.
22. J.Y. Xiang, J.P. Tu, L. Zhang, Y. Zhou, X.L. Wang, S.J. Shi, *Journal of Power Sources*, 195 (2010) 313-319.
23. Z. Wang, F. Su, S. Madhavi, X.W. Lou, *Nanoscale*, 3 (2011) 1618-1623.